

Numerical Study for Concentrated Photovoltaic Performance at Low Concentration Ratio

A. A. Harb^a, Khairy Elsayed^{b,c}, M. Sedrak^d

Department of Mechanical Power Engineering, Faculty of Engineering at El-Mattaria, Helwan University, Masaken El-Helmia P.O., Cairo 11718, Egypt

ABSTRACT

Concentrating photovoltaic (CPV) is an alternative technique used to convert the solar energy to electrical energy. CPV is used in lieu of the photovoltaic system (PV) due to its smaller semiconductor area and consequently lower cost. The study of fluid flow and thermal characteristics for a CPV integrated with a three dimensional (3D) rectangular shaped microchannel heat sink (MCHS) is numerically investigated. Laminar and steady flow of water as a coolant is used at the present study. The flow and thermal fields are analyzed using four channel number (N) (26, 52, 78 and 104), concentration ratio (CR) from 1 to 20 and Reynolds number (Re) from 100 to 1000. The evaluating parameters such as temperature, the electrical efficiency and the electrical power are obtained from the simulation. Results show that increasing the channel number over N equals 52 leads to a slight decrease in the cell temperature while the design of 26 channels achieves less cell temperature. As the concentration ratio increases, the cell efficiency decreases due to increase of the temperature while the electrical power increases. Increasing Re provides a negligible enhancement in the cell efficiency and consequently a slight increase in the electric power.

KEYWORDS

Concentrator photovoltaic, Microchannels, Heat sink, Numerical study, concentration ratio.

-
- a Teaching Assistant, Department of Mechanical Power Engineering, Faculty of Engineering at El-Mattaria, Helwan University, Masaken El-Helmia P.O., Cairo 11718, Egypt.
 - b Associate Professor, Department of Mechanical Power Engineering, Faculty of Engineering at El-Mattaria, Helwan University, Masaken El-Helmia P.O., Cairo 11718, Egypt.
 - c Mechanical Engineering Department, Arab Academy of Engineering and Technology and Maritime Transport, Smart Village Branch, Egypt.
 - d Professor, Department of Mechanical Power Engineering, Faculty of Engineering at ElMattaria, Helwan University, Masaken El-Helmia P.O., Cairo 11718, Egypt.

Nomenclatures

A	Solar cell Area (m ²)
c	Specific heat capacity (J/kg k)
D _h	Hydraulic diameter of the fluid flow channel (m)
G (t)	Net concentrated solar radiation (W/m ²)
H	Height or thickness (m)
k	Thermal conductivity (W/m K)
L	Microchannel length and solar cell length (m)
\dot{m}	Cooling fluid mass flow rate (kg/s)
N	Number of channels
P	Pressure (Pa), and Power (W)
Re	Reynolds number
T	Temperature (°C)
u, v, w	Velocity in x, y, and z direction (m/s)
W	Width, thickness of fin between flow channel and neighboring flow channel (m)
x, y, z	Cartesian coordinates

Greek Symbols

α	Absorptivity
β	Solar cell temperature coefficient (1/K)
ε	Emissivity
τ	Transmissivity
μ	Dynamic viscosity (kg/m s)
σ	Stephan-Boltzmann constant (5.67×10^{-8} (W/(m ² K ⁴))
ρ	Fluid density (kg/m ³)
δ	Thickness (m)
λ	Molecular mean free path (m)
η	Solar cell and thermal efficiency

Subscript

a	Ambient
b	Back sheet or tedlar
ch	Channel
conv, g-	Convection loss from glass to ambient
a	
el	Electrical
f	Fluid and fin spacing between the flow channel and the neighboring flow channel
fric.	Friction
g	Glass

in	Inlet
net	Net
out	Outlet
rad, g-s	Radiation loss from glass to sky temperature
ref	Reference condition, $G = 1000 \text{ W/m}^2$, $T=25^\circ\text{C}$
s	Sky
sc	Silicon wafer
th	Thermal
w	Wall and Wind

Abbreviations

CPV	Concentration photovoltaic system
CPV/T	Concentration photovoltaic thermal system
MCHS	Microchannel heat sink
PV	Photovoltaic

1. INTRODUCTION

Due to the decreasing in the fossil fuel, the solar energy demand is increased. One of the most promising techniques that is used to convert the solar radiation into electrical output is the photovoltaic (PV). However the large area of the semi-conductors used in the PV system make it very expensive. So an alternative technique is proposed to reduce the lager area of the semi-conductors and consequently its cost, called concentrator photovoltaic. The solar radiation is concentrated by mirrors and fall on the solar cells. The solar cell receives more radiation compared to the traditional PV system that leads to increase its temperature. The increase in the solar cell temperature significantly affects its performance by reducing the solar energy to electrical energy conversion and reducing the life time due to the degradation consequently. Thus an efficient cooling is needed to increase the solar cell efficiency. Chaudhari et al. (2014) considered the MCHS with water as coolant regarded an effective technology to reduce the solar cell temperature.

Wang et al. (2017) used a direct-contact liquid film for the cooling of an electric heating plate. The heating plate used as a PV solar cell. The CR ranged from 300X to 600X. The effect of the water inlet temperature and the flow rate at different values on the temperature uniformity and average cell temperature was studied. The results indicated that the difference between the maximum and the minimum temperature was acceptable. It was nearly 10°C . This ununiformed distribution is caused by the wavy flow of the film liquid. The increase in the flow rate has a slight effect on the temperature uniformity. Increasing the concentration ratio from 300X to 600X leads to an increase in the heat plate average temperature by 10°C and 5°C when the water inlet temperature was at 30°C and 75°C respectively.

Geng et al. (2012) performed a numerical and experimental investigation for the application of a heat pipe as a cooling technique for CPV system. The effect of operating parameters such as wind velocity and solar radiation were studied. Their results indicated that as the wind speed increases, the cell temperature decreases and the average temperature is 87 °C when the wind velocity is 10 m/s. Which exceed the upper limit for the normal operation of the CPV cell. Moreover it was found that if the heat flux is larger than 50 kW/m², the mean temperature is about 77 °C which is the upper limit. If the heat flux exceeds 50 suns, the used heat pipe heat dissipation system could not keep good operation conditions for the heat flux and additional heat pipes are required.

Recently, the CPV has become a very interesting topic to attract the researcher's attention. The application of microchannel heat sink has offered significant cooling performances for CPV. The study of flow and thermal fields for a steady and laminar flow was performed by Adham et al. (2016). The working fluid was a SiC-H₂O and TiO₂-H₂O nanofluids at different volume fractions passing through a rectangular channel. The optimization technique is used to minimize two objective functions, the first objective function is the total thermal resistance and the second is the pumping power. They reported that there are a decrease in the thermal resistance as the nanofluid concentration increases. Increasing the nanofluids concentration leads to an increase in the friction. Eventually, the pumping power is increased. Moreover, they indicated that increasing the aspect ratio (height/width) leads to a reduction in the thermal resistance and an increase in the pumping power. Different materials are used in that study. The result showed that for lowest thermal resistance the copper material is recommended while for light size and acceptable performance the aluminum material is recommended.

Radwan et al. (2016) studied the effect of the CR and the flow rate on the performance of the low CPV/T. It is found that the electrical efficiency reached approximately 18.5%, and the thermal efficiency achieves the maximum value of 62.5%, while the loss in the power due to microchannel friction is around 0.4% of the electrical power output. Also it is indicated that the microchannel has a significant effect on the solar cell temperature by decreasing its temperature from 62.1°C to 33.45°C at the maximum value of the solar radiation.

Tuckerman and Pease (1981) fabricated a micro-channel heat sink by chemically etching parallel channels in a 1-cm² silicon wafer. The channels had a width of 50 μm and a depth of 302 μm, and were separated by 50 μm thick walls. Using water as cooling fluid, they demonstrated that their micro-channel heat sink was capable of dissipating a heat flux of 790W/cm².

Xu et al. (2016) used the sequential quadratic programming technique to determine the optimum design of the MCHS. In that study, the thermal resistance was the objective function while the pressure drop was taken as one of the constraints. The results showed that the optimized microchannel number, layer, height, and width are 40, 2, 2.2 mm, and 0.2 mm, respectively, and its corresponding total thermal resistance for the whole MCHS was 0.0424 K/W. Also it is found that after optimizing the maximum temperature of the microchannel heat sink was reduced by 31.2 K with respect to the initial design. Also, it is revealed that the shorter channel leads to a smaller thermal resistance. It is clear that the good heat transfer property of heat sink is at the expense of a higher pumping power. Also it is found that as the aspect ratio and the number of channel increases the maximum temperature of the microchannel decreases asymptotically.

Du et al. (2012) experimentally compared CPV module with water cooling and fixed PV without cooling. The study was performed by evaluating the performance of the two systems for different performance parameters such as the efficiency, the power output and the temperature. The results showed that the maximum temperature difference between the CPV module and the fixed PV module was lower than 5 °C at 8.5 concentration ratio. Also it revealed that the electrical power of the CPV system was around 4.7 to 5.2 times higher than the fixed PV system. As the solar cell temperature increases, the solar to electrical efficiency decreases. Thus, at the solar noon the electrical efficiencies decrease for both PV systems. Since the solar cell of the CPV system receive more radiation, the electrical efficiency of the CPV was 7.81 % lower than that of the fixed PV module which was 10.68 %.

It should be noted from the above literature review that limited studies are available on the performance of CPV system integrated with a rectangular shaped MCHS and this has motivated the present study. Thus, the present study deals with 3D numerical simulations of laminar flow and heat transfer characteristics of rectangular shaped MCHS using water as a coolant. The channel number ranged from 26 to 104 and the Reynolds number ranged from 100 to 1000, and the CR ranged from 1 to 20 where CR equals unity means 1000 W/m² and CR equals 20 means 20 kW/m². Results of interests such as the average cell temperature, the electrical efficiency and the electrical power are the key parameters to illustrate the effects of channel number, Reynolds number and CR on the CPV performance.

2. MATERIALS AND METHODS

2.1. Physical Model

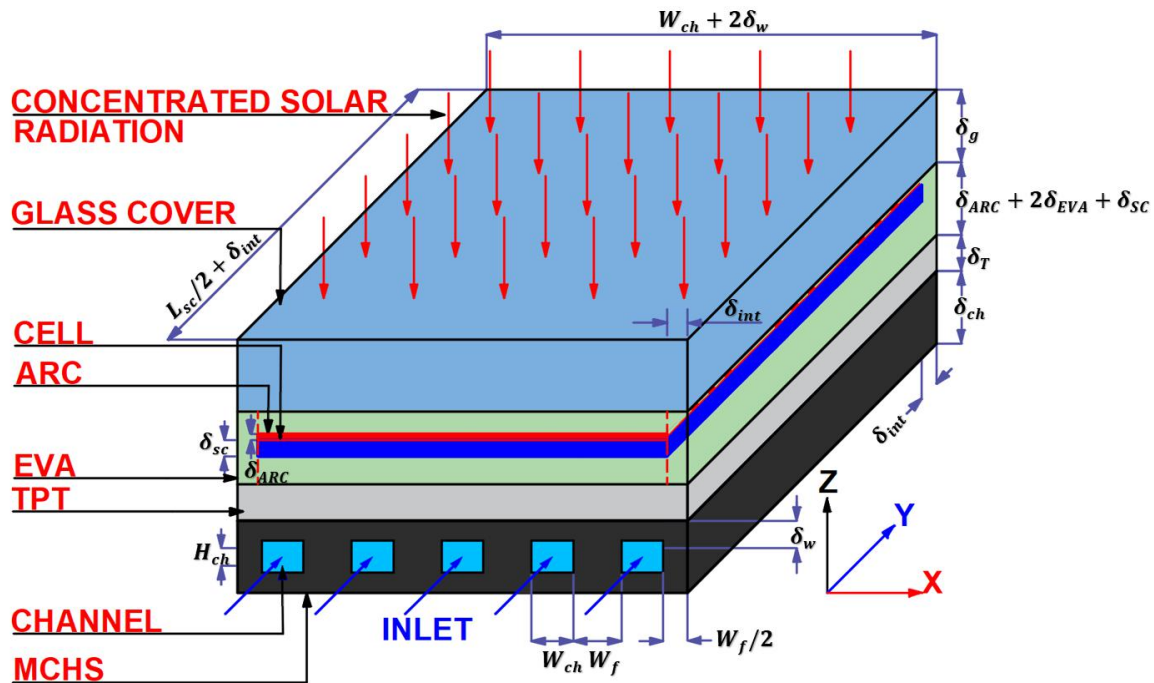


Fig.1: Schematic diagram and main dimensions of a CPV system integrated with MCHS.

The whole system of the CPV consists of a solar cell and a MCHS. Figure 1 shows the computational domain for the CPV integrated with MCHS. The upper surface of the system is exposed to the solar irradiation. The MCHS is located underneath the solar cell as shown in Fig. 1 and its function is cooling the solar cell. The entire system of the CPV consists of a series of the photovoltaic/thermal units in rows connected together in electrical manner. For this study a generic polycrystalline cell is used (King et al. 2004).

According to King et al. (2004), the manufacturing technology, there are a several layers for the solar cell as listed below:

1. Glass cover that has a 3 mm thickness and made of tempered glass with higher transparency.
2. An anti-reflective coating (ARC); to limit the reflection of the received radiation. This layer has a very small thickness of 0.0001 mm.
3. The solar cell (silicon layer); it is the layer that responsible for producing the electricity and made of 0.2 mm thickness silicon wafer (Singh et al. 2016). This layer is embedded in the ethylene vinyl acetate (EVA) layer.
4. An ethylene vinyl acetate (EVA) which is a transparent encapsulating material covers the silicon layer by 0.5 mm thickness above and below. The

functions of this layer are maintaining the silicon layer fixed, an electrical insulation and moisture resistance.

5. Tedlar polyester tedlar (TPT) which is made of polyvinyl fluoride material, has 0.3 mm thickness and it is an additional protection for the silicon layer from the moisture and also provide an electrical insulation (Armstrong 2010).

The expression of CR represents the average net solar irradiance of the concentrated beam falling on the solar cell area, relative to the reference value, that usually be “one-sun” value 1000 W/m^2 (Xu et al. 2014). As the CR increases the average solar irradiation incident on the PV system increase. For instance, if the CR equals 15, the average net solar flux incident on the solar cell area will be 15 kW/m^2 .

2.2. Theoretical Analysis

Three-dimensional fluid flow and heat transfer of the CPV system integrated with a rectangular aluminum MCHS were analyzed using water as the cooling fluid. Figure 1 shows a schematic structure and main dimensions of a CPV system integrated with MCHS. The dimensions are listed in Table 1 (Radwan et al., 2017).

Table 1. The dimensions of the PV system and MCHS.

Parameter	L_{sc}	H_{ch}	W_{ch}	δ_w	W_f	W_{sc}	$W_{ch,flat}$	N	δ_{ch}	δ_{int}
Value [mm]	125	0.1	0.8	0.2	0.4	125	126.8	106	0.5	1.1

Table 2. Numerical Assumptions

Parameters	Assumptions
Flow characteristics	Three dimensional, steady, incompressible , laminar and single phase
Body force	Neglected
Fluid properties	Temperature dependent (Siddiqui et al. 2013)
No slip boundary condition	$u = v = w = 0$ at solid wall (Patankar et al., 1980, Tao et al., 2001)
Inlet velocity	Uniform (Patankar et al., 1980, Tao et al., 2001)
Microchannels	Identical in heat transfer and flow characteristics (Xie et al., 2009)
Solar cell materials	Isotropic and temperature independent. (Siddiqui et al., 2013)
The thermal contact	Neglected (Siddiqui et al., 2013)

resistances

2.2.1. Governing equations

To model the heat transfer in the PV layers the energy equation is used as a governing equation, in addition, the continuity and the momentum equations to model the three-dimensional fluid flow and the heat transfer in the MCHS. To solve the governing equations, some assumptions should be considered. Following Radwan et al. (2017), the used assumptions and settings in this study are listed in Table 2. According to these assumptions, the conservation of mass, momentum and energy equations, respectively are as follows. These governing systems of equations described below were solved using the commercial CFD package, ANSYS-FLUENT 17.0.

2.2.2. PV-module layers

Following Radwan et al. (2017) and Siddiqui et al. (2013), the heat conduction equation for each solid layer in Cartesian coordinates system can be provided as follow:

$$\nabla \cdot (k_i \nabla T_i) + q_i = 0 \text{ and } i = 1, 2, \dots, 6 \quad (1)$$

where k_i is the thermal conductivity of the layer i , and q_i is the heat generation per unit volume of the layer i due to the absorption of the solar radiation. In this study, the value of i varies from 1 to 6 according to the solar cell layers which are the glass cover, upper EVA, ARC, silicon layer, lower EVA and finally the TPT layer, respectively. To calculate the value of q_i , for any layer the following equation is used as indicated in Zhou et al. (2015).

$$q_i = \frac{(1 - \eta_{sc}) G \alpha_i \tau_j A_i}{V_i} \quad (2)$$

where η_{sc} represents the solar cell electrical efficiency, α_i , A_i , and V_i are the absorptivity, the area, and the volume of the layer i , respectively; and finally, τ_j is the net transmissivity of layers above layer i .

The CPV system consists of different layers as mentioned before. In each layer the absorbed solar radiation is the source of the generated heat and this absorbed solar radiation is a function of the layer absorptivity. For all layers (except the silicon wafer), the absorbed solar radiation converts into heat, while for the silicon layer, the net absorbed solar irradiance is converted into electricity and heat depending on the electrical efficiency while the rest following this equation $((1 - \eta_{sc}) * Q_{et,abs,sc})$ is converted into heat.

To determine the heat generation per unit volume using Eq. (2), we substitute η_{sc} with zero (Zhou et al. 2015). The optical, thermophysical properties and dimensions for each layer are listed in Tables 3 and 4 respectively. Equation (3) can be used to calculate the solar cell efficiency.

$$(3)$$

where η_{ref} and β_{ref} represent the solar cell efficiency and temperature coefficient at a reference temperature of $T_{ref} = 25$ °C, respectively.

The value of η_{ref} and β_{ref} equals 0.12 and 0.0045 K⁻¹, respectively for polycrystalline silicon solar cell as reported by Sarhaddi et al (2010).

Table 3: Optical properties of CPV system layer (Zhou et al., 2015).

Material	Reflectivity	Absorptivity (α)	Transmissivity (τ)	Emissivity (ϵ)
Glass cover	0.04	0.04	0.92	0.85
EVA layer	0.02	0.08	0.90	—
Silicon Layer	0.08	0.90	0.02	—
Back sheet	0.86	0.128	0.012	0.9
Aluminum	—	—	—	0.9

Table 4: Thermophysical properties and thicknesses of CPV/T layers (Radwan et al., 2017).

Layer	Density (kg/m ³)	Specific heat (J/ kg K)	Thermal conductivity (W/ mK)	Thickness (mm)
Glass Cover	3000	500	2	3
ARC	2400	691	32	0.0001
Encapsulation (EVA)	960	2090	0.311	0.5
Silicon	2330	677	130	0.2
Tedlar	1200	1250	0.15	0.3
Microchannel (Aluminum)	2719	871	202.4	0.2

2.2.3. Microchannel Heat Sink

For a microchannel substrate, the heat conduction equation in the vector form without heat generation could be written as follow (Siddiqui, 2013):

$$\nabla \cdot (k_{ch} \nabla k_{ch}) = 0 \quad (4)$$

For microchannel heat sink, the fluid flow and energy equations of laminar, incompressible, and steady flow can be written in vector form as follows:

Mass conservation equation:

$$\nabla \cdot (\rho \vec{V}) = 0 \tag{5}$$

Momentum equations:

$$\vec{V} \cdot \nabla (\rho \vec{V}) = -\nabla P + \nabla \cdot (\mu \nabla \vec{V}) \tag{6}$$

Energy equation:

$$\vec{V} \cdot \nabla (\rho C_f T_f) = -\nabla \cdot (k_f \nabla T_f) \tag{7}$$

where the subscript f represents the fluid;

\vec{V} , P , μ , ρ , C_f , k_f , and T_f are the velocity vector, pressure, fluid viscosity, density, specific heat, thermal conductivity, and temperature. The variation of water’s thermophysical properties with temperature is considered using the higher ordered polynomial equations presented in Jayakumar (2007) due to the substantial changes that occur inside the microchannel, especially at higher CR values.

2.2.4. PV Characterizations

One of the important parameters to evaluate the CPV system performance is the electrical power produced by the CPV system, P_{el} . Equation (8) is used to calculate P_{el} as follows, (Emam et al., 2017):

$$P_{el} = \eta_{sc} \tau_g \beta_{sc} G(t) w_{sc} l_{sc} \tag{8}$$

where η_{sc} , τ_g , β_{sc} , $G(t)$, w_{sc} , l_{sc} are the solar cell efficiency, the glass transmissivity, the net concentrated solar radiation incident on the solar cell surface regardless of the concentrator’s optical losses, and the width and length of the solar cell, respectively.

2.2.5 Boundary Conditions

To solve the governing equations, the following boundary conditions must be identified:

- 1- For the PV layers, the thermal boundary condition for the upper wall of the glass layer is a combination of convection and radiation heat loss. The radiation heat loss is the heat lost between the cell glass cover and the atmosphere.
- 2- The adiabatic assumption is adopted for the side walls of the computational domain due to symmetry and the sides of the solar cell.
- 3- At channel inlet ($y=0$) the velocity component is determined for each Re Eq. (9). while $u=w=0$.
- 4- At the solid–fluid domains interface the no temperature jump boundary conditions as the Knudsen number, K_n , falls in the no-slip regime (i.e. K_n less than 0.001) (Dehghan et al., 2014). where K_n is the ratio of the molecular

mean free path length to the flow characteristic dimension which defined as follows:

$$Re = \frac{\rho_{in} V_{in} D_h}{\mu_{in}} \tag{9}$$

where $D_h = \frac{2(H_{ch} \times W_{ch})}{(H_{ch} + W_{ch})}$ is the hydraulic diameter

$$K_n = \frac{\lambda}{D_h} \text{ and} \tag{10}$$

- 5- $Re < 2200$ to keep the flow within laminar flow regime.
- 6- The fluid temperature at the channel inlet is assumed to be uniform.

In more details, the boundary conditions for the cooled CPV system integrated with MCHS are presented as follows:

The PV layers:

For upper side of the glass cover (Siddiqui, 2013):

$$\frac{0}{z} \leq x \leq (\delta_{ch} + \delta_{TSC} + 2\delta_{EVA}^{int}) \text{ and } 0 \leq y \leq (L_{sc} + \delta_g^{int}), \text{ and} \tag{11}$$

$$k_g \frac{\partial T}{\partial z} = h_{rad.g-s}(T_g - T_s) + h_{conv.g-a}(T_g - T_a)$$

where $h_{rad.g-s}$ is the equivalent radiative heat transfer coefficient and determined using Eq. (13) and $h_{conv.g-a}$ represents the convective heat transfer coefficient and estimated using Eq. (14) and T_s is the sky temperature and calculated from Eq. (15). For the glass cover, EVA, ARC, silicon, and tedlar sides, at the two planes parallel to the yz plane and are located at $x = 0$, $x = 2\delta_{int} + W_{sc}$ and $y = 0$ to $y = L_{sc} + 2\delta_{int}$ an adiabatic boundary condition is applied due to the symmetry as follows.

$$k_i \frac{\partial T}{\partial x} = 0 \tag{12}$$

$$h_{rad,g-s} = \frac{\sigma \epsilon (T_g^4 - T_s^4)}{(T_g + T_s)} \tag{13}$$

$$h_{con,g-a} = 5.82 + 4.07V_w \tag{14}$$

$$T_s = 298 - 0.0225 T_g \tag{15}$$

where k_i is the material thermal conductivity of layer i and its value varies from material to another as shown in Table 4. Similarly, at the planes parallel to the xz

plane and located at $y = 0$ and to $y = L_{sc} + 2\delta_{int}$ except the coolant inlet and outlet regions, an adiabatic boundary condition is assumed due to the symmetry.

$$k: \frac{\partial T}{\partial y} = 0 \tag{16}$$

For the solid-solid interfaces, a thermally coupled boundary condition is applied: at the glass cover-top EVA layer interface:

$$\begin{aligned} 0 \leq x \leq (W_{sc} + 2\delta_{int}), 0 \leq y \leq (L_{sc} + 2\delta_{int}), \text{ and} \\ k_{EVA} \nabla T_{EVA} = k_g \nabla T_g \end{aligned} \tag{17}$$

At the top EVA layer- ARC layer interface:

$$\begin{aligned} 0 \leq x \leq (W_{sc} + 2\delta_{int}), 0 \leq y \leq (L_{sc} + 2\delta_{int}), \text{ and} \\ k_{EVA} \nabla T_{EVA} = k_{ARC} \nabla T_{ARC} \end{aligned} \tag{18}$$

At ARC-silicon layer interface:

$$\begin{aligned} 0 \leq x \leq (W_{sc} + 2\delta_{int}), 0 \leq y \leq (L_{sc} + 2\delta_{int}), \text{ and} \\ k_{sc} \nabla T_{sc} = k_{ARC} \nabla T_{ARC} \end{aligned} \tag{19}$$

At silicon layer – bottom EVA interface:

$$\begin{aligned} 0 \leq x \leq (W_{sc} + 2\delta_{int}), 0 \leq y \leq (L_{sc} + 2\delta_{int}), \text{ and} \\ k_{EVA} \nabla T_{EVA} = k_{sc} \nabla T_{sc} \end{aligned} \tag{20}$$

At EVA- tedlar layer interface:

$$\begin{aligned} 0 \leq x \leq (W_{sc} + 2\delta_{int}), 0 \leq y \leq (L_{sc} + 2\delta_{int}), \text{ and} \\ k_T \nabla T_T = k_{EVA} \nabla T_{EVA} \end{aligned} \tag{21}$$

At tedlar-aluminum channel interface:

$$\begin{aligned} 0 \leq x \leq (W_{sc} + 2\delta_{int}), 0 \leq y \leq (L_{sc} + 2\delta_{int}), \text{ and} \\ k_{AL} \nabla T_{AL} = k_T \nabla T_T \end{aligned} \tag{22}$$

For the microchannel heat sink design fluid domain:

At the channel inlet:

$$\begin{aligned} \delta_w \leq x \leq (W_{sc} + 2\delta_{int} - \delta_w), y = 0 \text{ and} \\ \delta_w \leq z \leq (\delta_w + H_{ch}) \end{aligned}$$

The mesh investigation is one of the important steps in the simulation. It concerned with the type and the sizes of the mesh intervals. The best size was selected according to a comparison between different sizes results. Accordingly, different levels of cell number are used (141552, 261180, 526175, 1.0012E6, 1.4202E6 and 2.3118E6). It is found that after the cell number of 1.4202E6 there is no significant change in the results, so it is selected to perform the validation process to save the computing time (see Fig. 2).

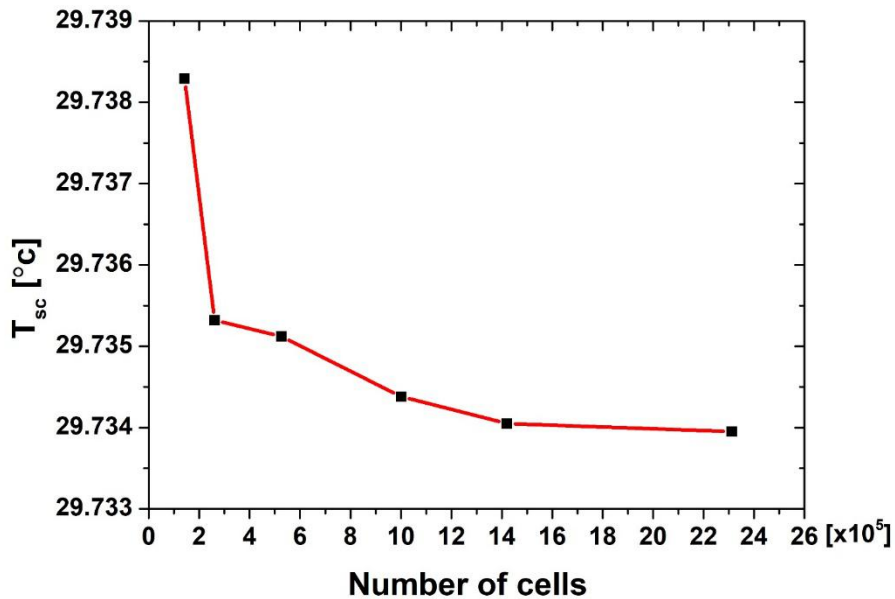


Fig. 2: Comparison between different levels of cell number.

Figure 3 presents a comparison between the results of the present numerical study, the numerical study of Radwan et al. (2017), and the experimental data of Baloch et al. (2015) for average temperature of the solar cell on 16th December. It can be seen that, the agreement between the numerical and the experimental results is acceptable. Therefore, the present numerical model is reliable and can be used to study the effect of channel number, the concentration ratio and Reynolds number on the performance of the solar cell.

The absorbed solar energy for all layers are convert to heat while the solar cell converts it to electricity and heat depending on the cell efficiency. The converted heat leads to increase the cell temperature and consequently reduce its efficiency. In order to minimize the temperature rise of the cell, the dissipation of heat with a high rate is necessary for their proper functioning. According to the literature review, MCHS have a significant effect on the cooling process. As a result, this study was carried out using MCHS with different numbers of channels namely (N) 26, 52, 78 and 104 and CR ranged from 1 to 20 at Reynolds number ranged from

100 to 1000. The CFD results present the influence of these parameters on the average solar cell temperature, the electrical efficiency and the electrical power.

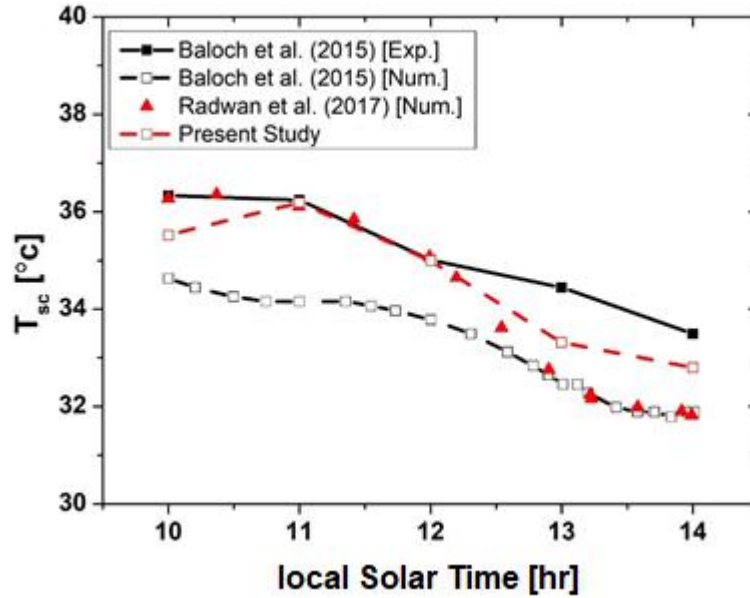


Fig. 3: Comparison of experimental and computational data and current prediction CFD results for solar cell average temperature at the local solar time of 10:14 and $Re = 530$.

The impact of increasing the channel number is numerically investigated in the present study. Figure 4 shows a schematic diagram of the computational domains of PV integrated with different MCHS configurations. The difference between these configurations was in the channel number. Table 5 shows the dimensions for the four configurations within the range of the literature (Radwan et al., 2017, Xu et al., 2016 and Tuckerman and Pease, 1981).

Table 5: The dimensions of different designs for the MCHS in [μm]

Model	L_{sc}	W_{sc}	W_{ch}	H_{ch}	N	δ_w	W_f	δ_{ch}	δ_{int}
1	125000	125000	710	823.3	104	526.67	513.077	1876.67	1100
2	125000	125000	710	823.3	78	526.67	920.769	1876.67	1100
3	125000	125000	710	823.3	52	526.67	1736.154	1876.67	1100
4	125000	125000	710	823.3	26	526.67	4182.308	1876.67	1100

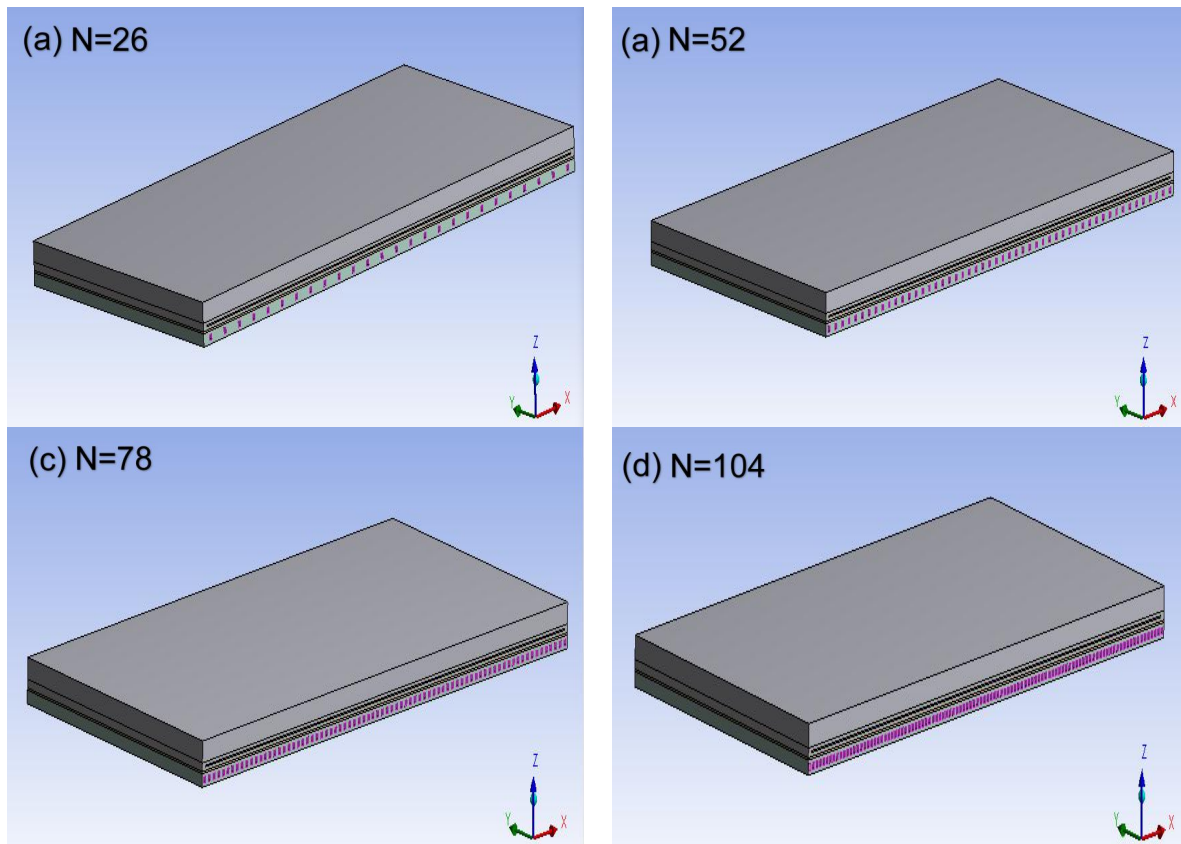


Fig. 4: Schematic diagram of the computational domains of PV integrated with different MCHS (a) N=26, (b) N=52, (c) N=78 and (d) N=104.

A comparison between different cell numbers for each design is performed. Table 6 indicates the mesh independent study only for last three samples (b, c and d) all designs of the MCHS.

Figure 5 shows the temperature contours for the solar cell at different channel number. For fair comparison of the contours of the cell section for the different design is obtained at the same range of temperature. It is clear that the channel number of 26 achieves the lowest solar cell temperature while the design of the N equals 52 achieves the highest value of 33.36°C . Moreover, Fig. 6 shows that increasing the channel number from 26 to 52 leads to an increase in the solar cell temperature by approximately 5.98°C while increasing the channel number after 52 leads to a slight decrease in the cell temperature.

N=26		N=52		N=78		N=104	
Cell Number	T [°C]	Cell Number	T [°C]	Cell Number	T [°C]	Cell Number	T [°C]
704885	27.766 7	1116810	33.3771 8	1510956	33.250 6	3978470	33.1407 5
925131	27.843	1234106	33.3565	1562760	33.250 6	4072010	33.1285 5
131652	27.807 7	2032627	33.3688	2253627	33.237 5	7504252	33.0924

Table 6: The mesh independent study for the four designs of the MCHS at $Re=100$.

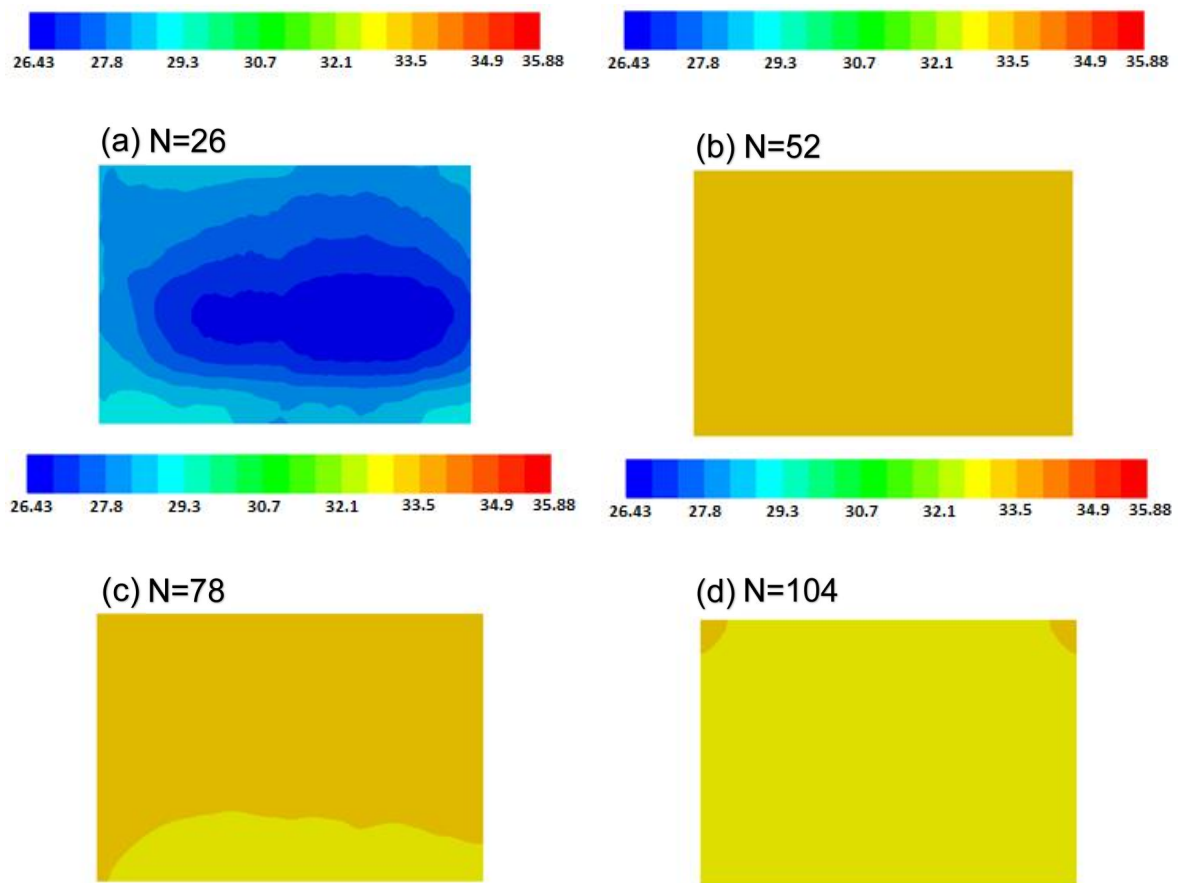


Fig. 5: Temperature contours for the solar cell at different channel number at $Re=100$.

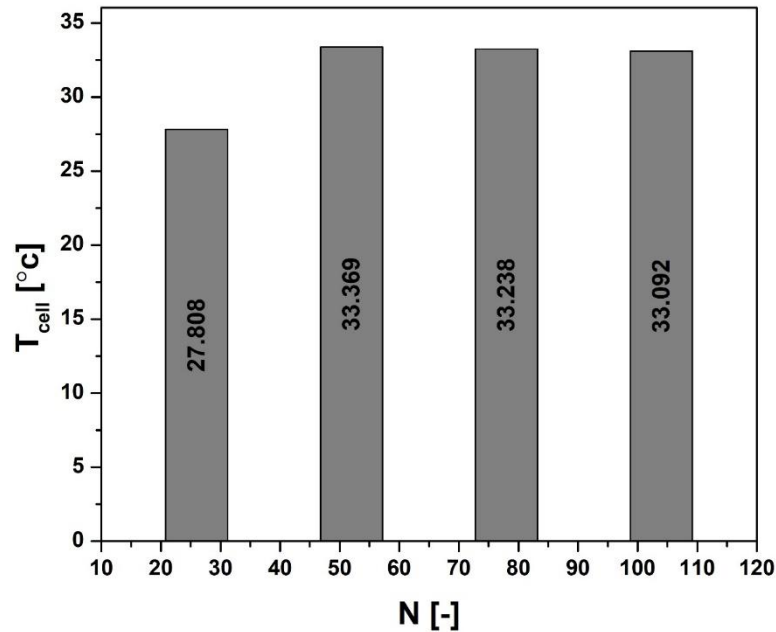


Fig. 6: The solar cell temperature versus the different channel number, at Re=100.

The effect of CR and Re is investigated computationally. The design of N equals 104 is selected for the rest of the present study due to the increased N achieves better temperature uniformity as reported by Radwan et al., (2017). Figure 7 depicts the effect of CR and Re on the average temperature for the solar cell for N=104. Generally, it is found that the influence of CR is significant while there are a little change by changing the Reynolds number. Based on Table 7, when the CR increases from 1 to 20, the solar cell temperature increases by 33.79%. Whereas at constant CR increasing the Reynolds number from 100 to 1000 leads to a slight reduction in the cell temperature by 1.56 °C equivalent to 1.8%.

Table 7: The dimensionless solar cell temperature versus CR at different Reynolds number of different designs for the MCHS

Re	T_{sc}/T_{in}				
	CR=1	CR=5	CR=10	CR=15	CR=20
100	1.104	1.477	1.942	2.408	2.874
200	1.103	1.472	1.932	2.393	2.853
300	1.102	1.468	1.924	2.381	2.838
400	1.1019	1.466	1.922	2.377	2.833
1000	1.101	1.464	1.916	2.369	2.822

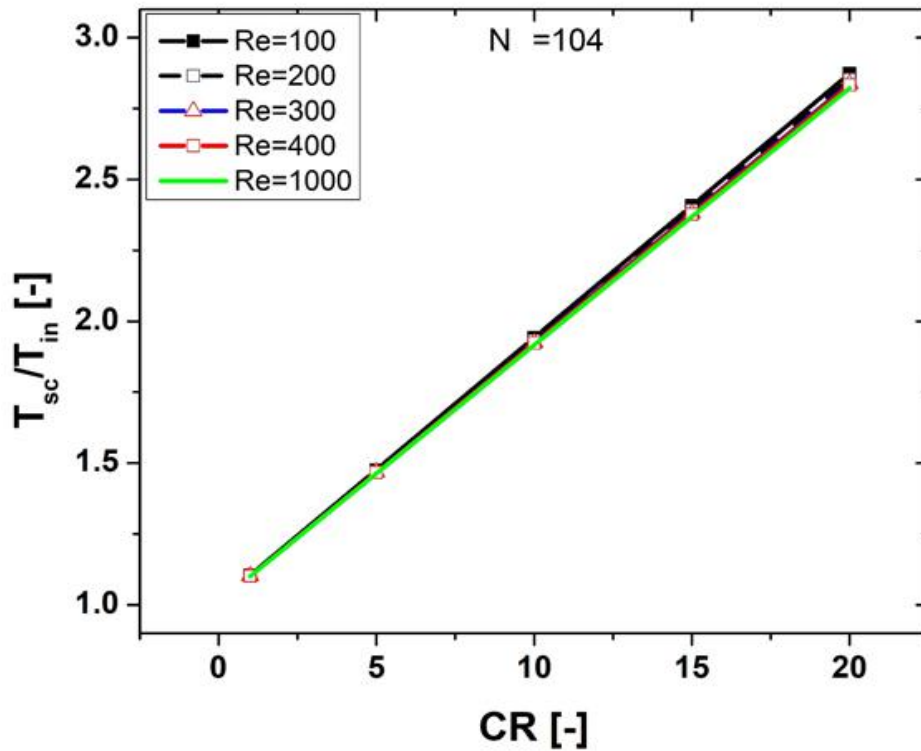


Fig. 7: Variation of the solar cell with the concentration ratio at different Re for N=104.

The main important performance parameters for the CPV systems are the electrical efficiency and the produced electrical power. Figure 8a, shows the effect of both the CR and Re on the electrical efficiency. It is clear that as the concentration ratio increases, the electrical efficiency decrease due to increasing the cell temperature. For example at Re=400 and CR= 1, 5, 10, 15 and 20 the corresponding values for the electrical efficiency is 11.56, 10.97, 10.236, 9.5 and 8.76 respectively. While increasing Re leads to a slight increase in the electrical efficiency due the enhancement of the cooling process. For instance at CR= 20 and Re= 100, 200, 300, 400 and 500 the electrical efficiency is 8.6947, 8.7274, 8.73515, 8.76 and 8.778 respectively.

In contrary the electrical power is significantly increases as the CR increases due to increasing the amount of the incident radiation on the solar cell. Also there are a slight increase in the electrical power as the Re increase where the electrical efficiency increases as Re increase and consequently the produced power increase as indicated in Fig. 8b.

(a)

(b)

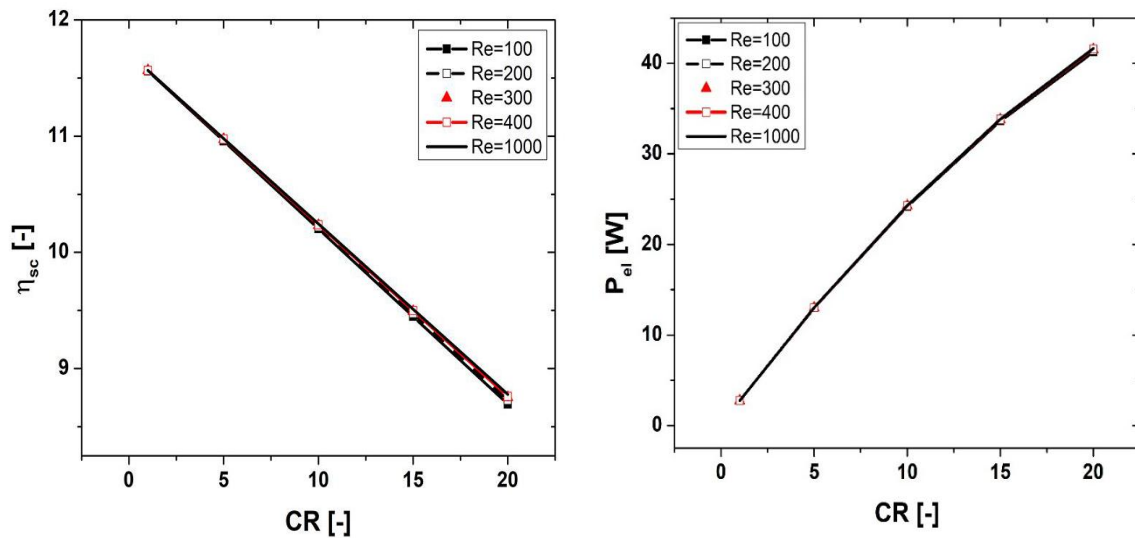


Fig. 8: The effect of CR and Re on a) the solar cell efficiency and b) the electrical power for N=104

5. CONCLUSIONS

A computational model was utilized to simulate a three dimensional fluid flow and heat transfer for a 3D CPV integrated with MCHS filled with water as a coolant. Based on the present computational study, the following results may be concluded:

- Increasing the channel number over N equals 52 leads to a slight decrease in the cell temperature while using N equals 26 gives the lowest cell temperature;
- As the CR increases the cell efficiency decreases due to the increase of the cell temperature, while the electrical power increase;
- Increasing Re from 100 to 1000 at N equals 104 showed unremarkable enhancement in the cell efficiency and consequently a slight increase in the electric power;
- It is recommended to apply the present results on actual CPV typical unit in collaboration with expert world-wide manufactures.
- According to the remarkable reduction in the cell temperature at N equals 26, the deep study for the channel number less than 26 is required.

REFERENCES

- Adham, A.M., Mohd-Ghazali, N. and Ahmad, R., 2016. Optimization of nanofluid-cooled microchannel heat sink. *Thermal Science*, 20(1), pp.109–118.
- Ahmed M, Eslamian M. 2014. Natural convection in a differentially-heated square

en- closure filled with a nanofluid: significance of the thermophoresis force and slip/ drift velocity. *Int Commun Heat Mass Transf*;58:1–11.

- Baloch, A. A. B., Bahaidarah, H. M. S., Gandhidasan, P., and Al-Sulaiman, F. A. 2015. Experimental and numerical performance analysis of a converging channel heat exchanger for PV cooling. *Energy Conversion and Management*, 103, 14–27.
- Chaudhari, K.S. and Walke, P. V., 2014. Applications of nanofluid in solar energy – A Review. *International journal of engineering research and technology*, 3(3), pp.460–463.
- Cordeiro, D. and Palma, C., 2013. – Laboratory of nano and microfluidics and micro-Sistems - LabMEMS, Mechanical Eng.Dept. - POLI and COPPE/UFRJ, Rio de Janeiro, Brazil 2 – Mechanical Engineering Coordination - CEFET-RJ, Itaguaí, Brazil. , (Cobem), pp.7827–7839.
- Du, B. 2012. Water cooled concentrated photovoltaic system. *Renewable and Sustainable Energy Reviews*, 16(9), pp.6732–6736.
- Dehghan M, Daneshipour M, Valipour MS, Rafee R, Saedodin S. 2015. Enhancing heat transfer in microchannel heat sinks using converging flow passages. *Energy Convers Manage*;92:244–50.
- Emam M, Ookawara S, Ahmed M. 2017. Performance study and analysis of an inclined concentrated photovoltaic-phase change material system. *Solar Energy*;150:229–45.
- Geng, W.G. 2012. Numerical and experimental study on cooling high-concentration photovoltaic cells with oscillating heat pipe. *International Journal of Low-Carbon Technologies*, 7(3), pp.168–173.
- Jayakumar JS, Mahajani SM, Mandal JC, Vijayan PK, Bhoi R. 2008. Experimental and CFD estimation of heat transfer in helically coiled heat exchangers. *Chemical Engineering Research and Design*;86:221–32.
- Ju X, Xu C, Han X, Du X, Wei G, Yang Y. 2017. A review of the concentrated photovoltaic/ thermal (CPVT) hybrid solar systems based on the spectral beam splitting technology. *Appl Energy*;187:534–63.
- King, D. L., Boyson, W. E., and Kratochvill, J. A. 2004. Photovoltaic array performance model, (December).
- Lokeswaran, S., Mallick, T.K. and Reddy, K.S., 2015. Thermal performance of a solar concentrating photovoltaic module with spiral mini channel heat sink. *International Conference on Polygeneration technologies and perspectives (ICP 2015)*, (February), pp.1–10.

- Mohd-Ghazali, N. et al., 2014. Optimization of square and circular ammonia-cooled microchannel heat sink with genetic algorithm. *Energy Procedia*, 61, pp.55–58.
- Radwan, A., Ahmed, M. and Ookawara, S., 2016. Performance enhancement of concentrated photovoltaic systems using a microchannel heat sink with nanofluids. *Energy Conversion And Management*, 119, pp.289–303.
- Radwan, A., Ookawara, S. and Ahmed, M., 2016. Analysis and simulation of concentrating photovoltaic systems with a microchannel heat sink. *Solar Energy*, 136, pp.35–48.
- Radwan, A. and Ahmed, M. 2017. The influence of microchannel heat sink configurations on the performance of low concentrator photovoltaic systems. *Applied Energy*, 206(May), 594–611.
- S.V. Patankar, 1980. Numerical Heat Transfer and Fluid Flow., Hemisphere, NY.
- Sarhaddi, F., Farahat, S., Ajam, H., Behzadmehr, A., and Adeli, M. M. 2010. An improved thermal and electrical model for a solar photovoltaic thermal (PV / T) air collector. *Applied Energy*, 87(7), 2328–2339.
- Siddiqui MU, Arif aFM. 2013. Electrical, thermal and structural performance of a cooled PV module: transient analysis using a multiphysics model. *Applied Energy*;112:300–12.
- Wang, Y. et al., 2017. Experimental study on direct-contact liquid film cooling simulated dense-array solar cells in high concentrating photovoltaic system. *Energy Conversion and Management*, 135, pp.55–62.
- W.Q. Tao, 2001. Numerical Heat Transfer, second ed., Xi'an Jiaotong University Press, Xi'an, China.
- W. Qu and I. Mudawar, 2002. Experimental and numerical study of pressure drop and heat transfer in a single-phase micro-channel heat sink, *International Journal of Heat and Mass Transfer* 45, pp. 2549-2565.
- Xu, S. 2016. Optimization of the thermal performance of multilayer silicon microchannel heat sinks. , *Thermal Science*, 20(6), pp.2001–2013.
- Xu, Z. and Kleinstreuer, C., 2014. Computational analysis of nanofluid cooling of high concentration photovoltaic cells. *Journal of Thermal Science and Engineering Applications*, 6(3), p.31009.
- Xu, Z. and Kleinstreuer, C., 2014. Concentration photovoltaic-thermal energy co-generation system using nanofluids for cooling and heating. *Energy Conversion and Management*, 87, pp.504–512.

- X. L. Xie, Z. J. Liu, Y. L. He and W. Q. Tao, 2009. Numerical study of laminar heat transfer and pressure drop characteristics in a water-cooled minichannel heat sink, *Applied thermal engineering*, vol. 29 , pp. 64-74.
- Yang, K. and Zuo, C., 2015. A novel multi-layer manifold microchannel cooling system for concentrating photovoltaic cells. *Energy Conversion And Management*, 89, pp.214–221.
- Zhou J, Yi Q, Wang Y, Ye Z. 2015. Temperature distribution of photovoltaic module based on finite element simulation. *Solar Energy*;111:97–103.